discerned for the poly-NiT(PCP)P film.

It is interesting to note that the poly-Ni- and -Co-paracyclophanylporphyrin films, as well as the poly-Ni- and -Co-[p-(diethylamino)phenyl]porphyrin films, manifest greater catalytic ability in the oxidation of hydrazine than the Ni-phthalocyanines and the Ni and Co tetrasulfonated phthalocyanines of ref 17. On the other hand, while the MnT(PCP)P and the Mn(p-Et_2N)TPP films demonstrate the least activity in the oxidation of hydrazine, both the Mn(Pc) and the Mn(TSP) exhibit the greatest activity in this oxidation reaction.[17a]

The thin T(PCP)P film, as seen in the scanning electron micrograph, Figure 4, is characterized by a smooth but irregular film morphology with no microspheroidical features and exhibits the least catalytic activity in the oxidation of hydrazine. Although the thicker, caramellike surface of the Ru(CO)(p-Et_2N)TPP(t-Bupy) film, Figure 5a, appears relatively smooth, it contains many craters that are characterized by a compact microspheroid surface morphology, Figure 5b, and catalytically exhibits a medium-range activity in the hydrazine oxidation reaction. Contrasting with these two films is the film of Co(p-Et_2N)TPP, Figure 6, which is rougher with no craters present and exhibits a very high catalytic activity in this oxidation process. Interestingly, the surface morphology of these three films correlates very well with the double-layer capacitance (C_{dl}) data obtained from some impedance spectroscopy measurements.[32] These data demonstrate unusually large C_{dl} values, indicating the presence of quite intricate and rough film surfaces. It would be worthwhile, at this point, to examine the film morphologies of both the free-base and metalated PCPP films, the other metalated T(PCP)P films, and the remaining metalated (p-Et_2N)-TPP films, to see if their surface morphologies parallel the catalytic activity in this particular oxidation reaction.

Conclusions

The results obtained from the catalytic studies presented in Tables II and III clearly demonstrate that the paracyclophanylporphyrin film electrodes and the [p-(diethylamino)phenyl]porphyrin film electrodes play a significant role in the electrocatalytic oxidation of hydrazine.

For the paracyclophanylporphyrin films, PCPP, CoPCPP, CoT(PCP)P, and the NiT(PCP)P all exhibit large ΔE values that range from 400 to 630 mV. Similarly, with the [p-(diethylamino)phenyl]porphyrin films, Co(p-Et_2N)TPP and the Ni(p-Et_2N)TPP manifest the most negative anodic peak potentials, resulting in ΔE values ranging from 520 to 680 mV. Unequivocally, both the Co and Ni paracyclophanylporphyrin films and the Co- and Ni-[p-(diethylamino)phenyl]porphyrin films demonstrate catalytic capabilities in this reaction. The surface morphology of the films discussed also suggest features that may be important in their catalytic activity, especially in the oxidation of hydrazine.

Acknowledgment. We acknowledge and thank Professor Czuchajowski et al., Department of Chemistry, University of Idaho, Moscow, Idaho, for the original synthesis and generous supply of the free-base and metalated paracyclophanylporphyrins.

Registry No. PCPP (homopolymer), 121749-05-1; CoPCPP (homopolymer), 132911-79-6; T(PCP)P (homopolymer), 123785-92-2; MnT(PCP)P (homopolymer), 132938-13-7; CoT(PCP)P (homopolymer), 132938-14-8; NiT(PCP)P (homopolymer), 132938-15-9; Co(p-Et_2N)TPP (homopolymer), 123833-36-3; Ni(p-Et_2N)TPP (homopolymer), 133099-45-3; Ru(CO)(p-Et_2N)-TPP(t-Bupy) (homopolymer), 123833-38-5; Mn(p-Et_2N)TPP (homopolymer), 132938-16-0; hydrazine, 302-01-2.

Composition-Controlled Metal–Nonmetal Transition in $La_{2-x}Sr_xNiO_{4-\delta}$

C.-J. Liu, M. D. Mays, D. O. Cowan,* and M. G. Sânchez*

Department of Chemistry, The Johns Hopkins University, Baltimore, Maryland 21218

Received December 12, 1990. Revised Manuscript Received March 4, 1991

Materials with the general composition $La_{2-x}Sr_xNiO_{4-\delta}$ retain the perovskite-related structure of space group $I4/mmm$ up to $x = 1.50$. They undergo a composition-dependent metal–nonmetal transition in electrical conductivity. The composition parameters x and δ determine the conductivity type. For $x < 1$ the materials are nonmetals. For $x > 1.1$ metallic conductivity is observed that persists to a limit of at least $x = 1.50$ if the oxygen deficiency δ is low. For compositions near the transition the conductivity type is also dependent on δ. Metallic samples become nonmetals upon heating in flowing Ar at 1000 °C, which revert to metals upon oxidation in O_2 also at 1000 °C. All nonmetal-to-metal transitions are accompanied by a change in color from black to reddish brown. The Ni average valence v was determined from the metals composition and iodometric titration data. The δ value was calculated from v by using the equation $\delta = 0.5x + (1 - 0.5v)$, which was derived by using a formal valence convention. Both v and δ increase monotonically with x in the range $0 \leq x \leq 1.5$. A phase diagram is proposed for the metal–nonmetal transition in which the boundary is given by $\delta = 0.5x - 0.51$, which corresponds to $v \approx 3.02$. No stoichiometric 214 nickelate ($\delta = 0$) could be prepared in the metallic region, and no superconductive transition was observed in any material down to ~3 K.

Introduction

Many efforts have been made to increase the transition temperature, T_c, of the ceramic superconductive cuprates and to understand the nature of the new type of conductivity shown by these new materials. One of the tactics used has been to substitute the ionic metals by similar metals. These substitutions preserve the –[CuO_2]– layers within the structure, but they change the interatomic distances as well as the charge carrier concentration and type. Another tactic has been to use other transition metals in the square-planar array. One candidate for this type of approach is $La_{2-x}Sr_xNiO_{4-\delta}$, which is known to form

0897-4756/91/2803-0495$02.50/0

the 214 analogue series in the range $0 \leq x \leq 1$. This series has been the object of numerous studies before and after the discovery of the high-T_c superconductors $La_{2-x}Ba_xCuO_{4-\delta}$[1] and $La_{2-x}Sr_xCuO_{4-\delta}$[2]. The end member of the series ($x = 0$) was reported by Rabeneau[3] in 1958 and by Müller-Buschbaum[4] in 1978 to be tetragonal with $I4/mmm$ space group symmetry. Ganguly[5] in 1973 reported a gradual semiconductor–metal transition near 500 K without any apparent structural change. In 1984 Rao[6] reported results obtained on single crystals prepared by the skull melting technique that confirmed the tetragonal symmetry using X-ray diffraction (XRD) methods. However, electron diffraction patterns exhibited superlattice reflections corresponding to a $\sqrt{2}a$ type of unit cell. The presence of excess, interstitial oxygen and resulting Ni^{3+} were implicated in the slight distortions observed in the crystalline framework. In 1976 Demazeau[7] reported the synthesis of $LaSrNiO_{4-\delta}$, which was annealed in oxygen at 900 °C at "ordinary" pressure and at 600 °C at 2 kbar. Iodometric titrations showed hypostoichiometric oxygen ($\delta > 0$) following the low-pressure annealing, implying the presence of some Ni^{2+}, and the high-pressure annealing produced stoichiometric oxygen level corresponding to a Ni valence of 3.00 ± 0.02. Stoichiometric $LaSrNiO_4$ ($\delta = 0$) was found to exhibit nonmetallic character. A detailed structural characterization of $La_2NiO_{4+\delta}$ has been published by Jorgensen et al.[8] using Rietveld refinement of neutron diffraction data. They report remarkable similarities between the nickelate and the $La_2CuO_{4+\delta}$ system;[9] both exhibit interstitial oxygen defects. Kakol and coworkers[10] have reported observing superconductivity in a fraction of the material $La_{2-x}Sr_xNiO_4$ with transition temperatures of up to 70 K. Later work by Kakol[11] provides evidence for the coexistence of superconductivity and antiferromagnetism in pure La_2NiO_4 below the onset temperature of 69 K in a small fraction of the sample. Ganguli et al.[12] report that while there is clear onset of diamagnetism around 20 K in many of the nickelates, they do not, however, find any anomaly in resistivity, magnetoresistance, or thermopower at 20 K. Thus, we witness over about 30 years studies beginning with the end member of the series (La_2NiO_4) and subsequent modifications involving the presence of oxygen defects (interstitial excess as well as vacancies); the doping with Sr and the oxidation of Ni; the elimination of vacancies using high oxygen pressure in the $LaSrNiO_4$, forming Ni^{3+}, and various combinations of these.

In this paper we report the crystal structure and electron-transport properties of $La_{2-x}Sr_xNiO_{4-\delta}$ for $0 \leq x \leq 1.50$.

Table I. Unit Cell Parameters for $La_{2-x}Sr_xNiO_{4-\delta}$ Body-Centered Tetragonal ($I4/mmm$)

composition	a, Å	c, Å	V, Å^3	c/a
$La_2NiO_{4-\delta}$[a]	3.865	12.630	188.7	3.268
$La_{1.90}Sr_{0.10}NiO_{4-\delta}$	3.854	12.703	188.7	3.296
$La_{1.90}Sr_{0.10}NiO_{4-\delta}$[a]	3.854	12.646	187.8	3.280
$La_{1.80}Sr_{0.20}NiO_{4-\delta}$[a]	3.846	12.683	187.6	3.298
$La_{1.70}Sr_{0.30}NiO_{4-\delta}$[a]	3.836	12.699	186.9	3.310
$La_{1.50}Sr_{0.50}NiO_{4-\delta}$[a]	3.817	12.766	186.0	3.345
$La_{1.50}Sr_{0.50}NiO_{4-\delta}$	3.813	12.754	185.4	3.345
$La_{1.40}Sr_{0.60}NiO_{4-\delta}$[a]	3.817	12.717	185.3	3.332
$La_{1.33}Sr_{0.67}NiO_{4-\delta}$	3.812	12.673	184.1	3.325
$La_{1.30}Sr_{0.70}NiO_{4-\delta}$[a]	3.821	12.689	185.2	3.321
$La_{1.20}Sr_{0.80}NiO_{4-\delta}$[a]	3.820	12.645	184.5	3.310
$La_{1.10}Sr_{0.90}NiO_{4-\delta}$[a]	3.821	12.590	183.8	3.295
$La_{1.00}Sr_{1.00}NiO_{4-\delta}$[a]	3.821	12.550	183.2	3.284
$La_{1.00}Sr_{1.00}NiO_{4-\delta}$	3.829	12.452	182.6	3.252
$La_{1.00}Sr_{1.0}NiO_{4-\delta}$[b]	3.826	12.450	182.2	3.254
$La_{0.90}Sr_{1.10}NiO_{4-\delta}$	3.829	12.423	182.1	3.245
$La_{0.85}Sr_{1.15}NiO_{4-\delta}$	3.832	12.388	181.9	3.233
$La_{0.80}Sr_{1.20}NiO_{4-\delta}$	3.834	12.382	182.0	3.229
$La_{0.70}Sr_{1.30}NiO_{4-\delta}$	3.831	12.346	181.2	3.223
$La_{0.60}Sr_{1.40}NiO_{4-\delta}$	3.829	12.339	180.9	3.223
$La_{0.50}Sr_{1.50}NiO_{4-\delta}$	3.824	12.335	180.4	3.225

[a] Reference 13. [b] Reference 7.

In the range $0 \leq x \leq 1.00$ we have done limited work duplicating earlier studies in order to establish the validity of our preparation and characterization methods and to provide the basis for trend analysis. Our main area of interest is the composition range $x > 1$, which has not been reported in the literature. The possible formation of materials comprising tetravalent nickel while maintaining $I4/mmm$ symmetry was of major interest. While we recognize that other formalisms may be used, we have elected to describe our work in terms of the formal valence states of Ni. For mixed valence systems we shall often speak of the average Ni valence v. Under this convention, v may be expressed as a function of x and δ and the formal valences of La, Sr, and O.

Experimental Section

Several members of the $La_{2-x}Sr_xNiO_{4-\delta}$ series in the range $0.1 \leq x \leq 1.6$ were prepared by coprecipitation of basic carbonates, followed by thermal decomposition and reaction in oxygen. The desired atomic ratios of La, Sr, and Ni were obtained by mixing quantitatively metal nitrate solutions of known assay. The mixed solution was then gradually added with strong agitation into a basic potassium carbonate solution containing excess potassium hydroxide. The resulting solids were filtered and water washed to remove undesirable electrolytes. The wash water had been previously saturated with hydrous La, Sr, and Ni basic carbonates. The washed solids were dried at 110 °C; the resulting pale green materials were fired in oxygen at 1375 ± 25 °C overnight, ground into powders, pelleted, sintered at 1375 ± 25 °C, and annealed in oxygen.

Powder X-ray diffraction data were obtained by using a Phillips APD-3720 automatic powder diffractometer over the range $5° \leq 2\theta \leq 80°$ in 2 h. The unit-cell parameters were computed and refined by using the APD-1700 crystallographic analysis software.

Electrical resistance as a function of temperature was measured by using a computer-controlled automated data collection system. Silver paste was used to make electrical contacts in a linear four probe configuration. The cooling (or heating) rate was typically 1 K/min. Data were collected at increments of about 0.1 K. The sample was mounted in a quasi-isothermal copper can, and the temperature was measured with a calibrated silicon diode.

Results

All our samples were virtually single phase with $I4/mmm$ space group symmetry. Some X-ray patterns showed at most three or four small unindexible peaks with $I/I_{max} < 3\%$, which appear to be due to a trace of NiO as

(1) Bednorz, T. G.; Müller, K. A. *Z. Phys.* **1986**, *B64*, 189.
(2) Tarascon, J. M.; Greene, L. H.; McKinnon, W. R.; Hull, G. W.; Geballe, T. H. *Science* **1987**, *235*, 1373.
(3) Rabeneau, A.; Eckerlin, P. *Acta Crystallogr.* **1958**, *11*, 304.
(4) Müller-Buschbaum, Hk.; Lehman, U. *Z. Anorg. Allg. Chem.* **1978**, *447*, 47.
(5) Ganguly, P.; Rao, C. N. R. *Mater. Res. Bull.* **1973**, *8*, 408.
(6) Rao, C. N. R.; Buttrey, D. J.; Otsuka, N.; Ganguly, P.; Harrison, H. R.; Sandberg, C. J.; Honig, J. M. *J. Solid State Chem.* **1984**, *51*, 266.
(7) Demazeau, G.; Pouchard, M.; Hagenmuller, P. *J. Solid State Chem.* **1976**, *18*, 159.
(8) Jorgensen, J. D.; Dabrowski, B.; Pei, S.; Richards, D. R.; Hinks, D. G. *Phys. Rev. B* **1989**, *40*, 2187.
(9) Jorgensen, J. D.; Dabrowski, B.; Pei, S.; Hinks, D. G.; Soderholm, B.; Morosin, B.; Shirber, J. E.; Venturini, E. L.; Ginley, D. S. *Phys. Rev. B* **1988**, *38*, 11337.
(10) Kakol, Z.; Spalek, J.; Honig, J. M. *J. Solid State Chem.* **1989**, *79*, 288.
(11) Kakol, Z.; Spalek, J.; Honig, J. M. *Solid State Commun.* **1989**, *71*, 283.
(12) Ganguli, A. K.; Nagarajan, R.; Ranga Rao, G. Vasanthacharya, N. Y.; Rao, C. N. R. *Solid State Commun.* **1989**, *72*, 195.

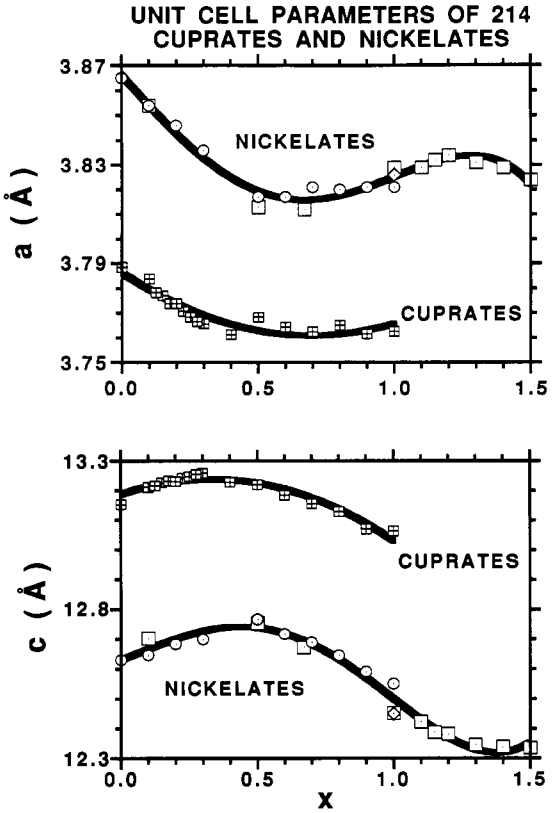

Figure 1. Experimental unit cell parameters a and c of the 214 La, Sr nickelates and cuprates as a function of metals composition (x). The data points for nickelates include the results of ref 13 (dotted circles), ref 7 (dotted diamonds) in the range $0 \leq x \leq 1$, and our data in the range $0 \leq x \leq 1.5$ (dotted squares). The crossed squares represent the published cuprate data.[2]

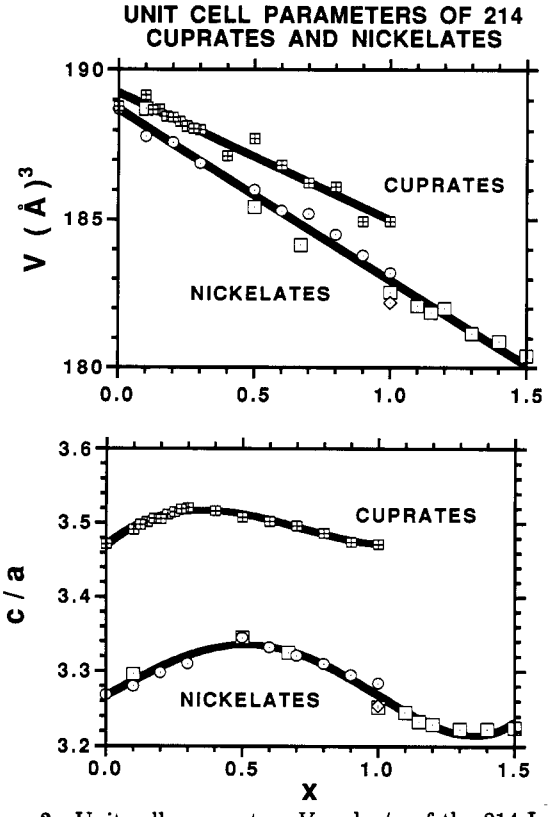

Figure 2. Unit cell parameters V and c/a of the 214 La, Sr nickelates and cuprates as a function of metals composition (x). The composition ranges and the symbols are the same as in Figure 1.

a second phase. In the range of primary interest the compositions corresponding to x = 1.10, 1.15, 1.20, 1.30, 1.40, and 1.50 showed respectively I/I_{max} = 0.9, 0.4, 0.7, 1.2, 0.7, and 0.9%. The X-ray pattern of the material with x = 1.60 indicated the presence of a second main crystal phase as yet unidentified. The limit of stability of the 214 crystal phase for the system was therefore placed somewhere in the range $1.50 < x < 1.60$.

The crystallographic data for $0 \leq x \leq 1$ of Gopalakrishnan et al.[13] and Demazeau[7] and our data in the range $0.1 \leq x \leq 1.5$ are summarized in Table I and shown in Figures 1 and 2. The XRD error limit of the parameters were in all cases under 0.0004 Å for a and 0.002 Å for c. The values given were rounded to three decimals to keep the data in line with those in the literature.

The average Ni valence was determined by dissolution of the sample in dilute hydrochloric acid containing potassium iodide followed by iodometric titration with sodium thiosulfate of known assay. The oxygen deficiency (δ) was calculated from

$$\delta = 0.5x + (1 - 0.5\upsilon) \quad (1)$$

which may be derived from the metals stoichiometry of the compound, the formal valences of La, Sr, and O, and the average Ni valence υ. We report the uncorrected data for υ and δ since the error introduced by trace levels of the NiO phase are minimal and do not affect the overall conclusions. Note that in a plot of δ vs x the slope of the line representing eq 1 will always be 0.5 and that the intercept $(1 - 0.5\upsilon)$ will be determined solely by the average Ni valence.

The samples in the range of $0 < x < 1$ were black. Beyond $x \approx 1$, the materials gradually changed to a dark brown color, and at x = 1.15 and beyond they developed a reddish hue. Ni^{4+} compounds are reddish in color (K_2NiF_6, Cs_2NiF_6).

Recognizing the uncertainty factors associated with resistivity measurements in polycrystalline materials, we chose to report electrical conductivity data in terms of relative resistance, which we defined as the resistance at temperature T divided by the resistance at 300 K. The original data typically included over 2000 experimental points for each material. The results on seven materials are shown in Figure 3. The upper graph shows the traces of three materials in the composition range $x \leq 1.03$. All exhibit nonmetallic type conductivity ($dR/dT < 0$). The lower graph shows the traces of four materials in the composition range $x \geq 1.15$. All exhibit metallic character ($dR/dT > 0$) in the range $100 \leq T \leq 300$ K, and all but the material with x = 1.15 retain the metallic character down to 10 K and show minimum resistance between 10 and ~3 K depending on the sample. The slopes of all plots between 300 and 100 K change monotonically with increasing Sr concentration.

Table II summarizes the key compositional parameters and some of the properties of the materials studied.

The changes in conductivity type and in oxygen deficiency (δ) in the transition compositional range led us to study in greater detail this region. Two separate studies were carried out.

The first study was on the effect of δ on the type of conductivity at constant metals composition. To do this, we placed two wafer chips from each of the materials with x = 1.15 and 1.20 in a tube furnace and simultaneously

(13) Gopalakrishnan, J.; Colsmann, G.; Reuter, B. *J. Solid State Chem.* **1977**, *22*, 145.

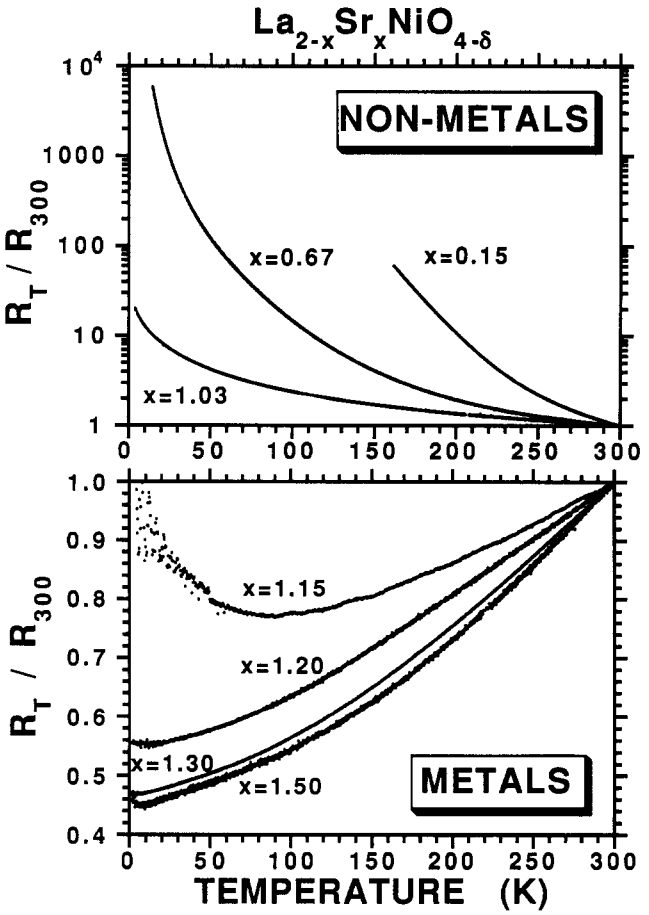

Figure 3. Relative resistance of La, Sr nickelates as a function of temperature for various metals compositions (x). The upper graph shows the data of three representative samples in the range of $0 < x < 1.03$ in which all materials are nonmetals. The lower graph shows the data from data samples in the range $1.15 \leq x \leq 1.50$. Their conductivity type is metallic in the range $1.2 \leq x \leq 1.5$ down to ~10 K. Note the overall monotonic increase of the slopes (dR/dT) as x increases.

Table II. Parameters and Properties of $La_{2-x}Sr_xNiO_{4-\delta}$

parameters			properties	
x	v^a	δ^b	color	conductivity type
0.10	2.330	−0.115	black	nonmetallic
0.15			black	nonmetallic
0.50			black	nonmetallic
0.67	2.655	0.006	black	nonmetallic
1.00			very dark	nonmetallic
1.03			very dark	nonmetallic
1.05			very dark	metallic
1.10	3.064	0.018	very dark	metallic
1.15	3.086	0.032	reddish brown	metallic
1.20	3.132	0.034	reddish brown	metallic
1.30	3.203	0.049	reddish brown	metallic
1.40	3.284	0.058	reddish brown	metallic
1.50	3.375	0.062	reddish brown	metallic

[a] Determined by iodometric titration. [b] Calculated from x and v by using eq 1.

heated them overnight in flowing Ar at 1000 °C and cooled them to ambient temperature also in Ar. One chip of each material was removed for relative resistance measurements. The other two chips were subsequently heated overnight in flowing oxygen at 1000 °C, cooled under oxygen, and removed for measurements. The results are shown in Figure 4.

In the second study, another group of wafers were prepared from the same powder precursors that had been previously used. All the preparation steps were carried

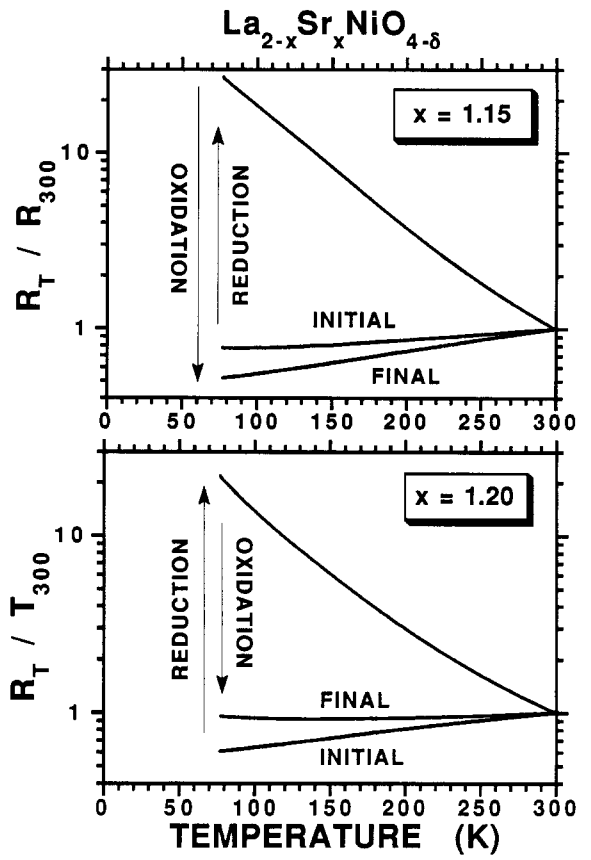

Figure 4. Changes in conductivity type at constant x brought about in materials near the compositional transition region (x = 1.15 and 1.20) by heating in argon (metal-to-nonmetal reduction) and then in oxygen (nonmetal-to-metal oxidation) at 1000 °C. The metal–nonmetal transitions are reversible.

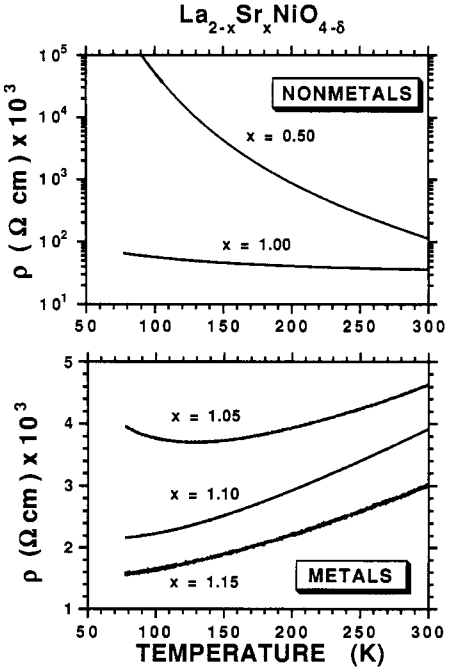

Figure 5. Resistivities of La, Sr nickelates as a function of temperature for various metals compositions (x). The upper graph shows the data of two representative samples in the range $0.5 \leq x \leq 1.0$. All materials are nonmetals. The lower graph shows the data of three samples in the range $1.05 \leq x \leq 1.15$. Their conductivity type is metallic.

out under the same nominal conditions used in the earlier work. The resulting wafers were carefully cut into orthogonal parallelepipeds, and their resistivities (ρ) were

measured down to 77 K. Plot of these approximate resistivities as a function of temperature are shown in Figure 5.

Discussion

The discussion that follows mainly addresses the major effects in electrical conductivity and crystal structure brought about by the changes in the composition (x) and by the level of oxygen vacancies (δ), which depends both on x as well as on the O_2 pressure during preparation. The $La_{2-x}Sr_xNiO_{4-\delta}$ series will be discussed whenever possible in relation to the $La_{2-x}Sr_xCuO_{4-\delta}$ isomorphous series, which has been studied very intensively and characterized in depth.

In the cuprate system, the Cu–O_{xy} distance in the square-planar array is ~1.89 Å, which is significantly smaller than the sum of the ionic radii (~2.09 Å), whereas the apical Cu–O_z distance (~2.42 Å) is appreciably larger than the sum of the radii. The dimensions in this elongated octahedron suggest that the bonding in the square-planar array is covalent in character and that the bonding between the –[Cu–O_2]– layers and their surroundings is mainly ionic. This view is supported by the studies of Pickett[14] and others on the charge density of La_2CuO_4 in which the La and the O_z are characterized as "essentially fully ionic" while a covalent character is assigned to the Cu–O_{xy} bonding in the square-planar array. In the nickelate system, the corresponding Ni–O_{xy} distance (~1.92 Å) is also smaller than the sum of the ionic radii (~2.12 Å for Ni^{2+} and ~2.02 Å for Ni^{3+}). This suggests that covalent bonding is also present to some degree. The Ni–O_z in La_2NiO_4 has been reported[8] as 2.261 Å (larger than the sum of the ionic radii) indicating a situation similar to the cuprate system but with significantly smaller octahedral distortion.

In both series the substitution of La^{3+} by Sr^{2+} removes valence electrons from the metal–oxygen octahedron which brings about the oxidation of Ni (Cu) or of O or a combination of both in order to maintain overall electrical neutrality. Whatever the case, the principal cause for the observed effects as x increases is a change in the electronic configurations between Ni (Cu) and O in the distorted octahedrons. The crystal structures provide valuable information on this important point, and the electrical properties reflect the changes in electronic configurations.

Over the entire composition range V (a^2c) decreases linearly with x in both systems, and for any given value of x the volumes are virtually the same (V_{Ni} is about 99.3 ± 0.3% of V_{Cu}).[2] However, the c/a parameters indicate that the cuprate cells are appreciably taller and thinner than the cells for nickelates. Both systems possess an important common characteristic. They exhibit opposite trends in the variations of the a and c edges as x increases. In the nickelates the a edge decreases for small values of x and goes through a minimum at $x \approx 0.6$, an inflection point at $x \approx 1$, and a maximum at $x \approx 1.3$, and the c edge goes through a maximum at $x \approx 0.5$, an infection point at $x \approx 1$, and a minimum at $x \approx 1.4$. This opposite trend in a and c is also observed in $Nd_{2-x}Sr_xNiO_{4+\delta}$[15] and the cuprate system in the range $x \leq 1$. These trends as well as the accompanying nonmetal–metal transition provide important information on the changes in electronic distribution around the Ni (or Cu) that are brought about by the removal of electrons from the metal–oxygen octahedron as La^{3+} is replaced by Sr^{2+}.

(14) Pickett, W. E. *Rev. Mod. Phys.* **1989**, *61*, 433.
(15) Arbuckle, B. W.; Ramanujachary, K. V.; Zhang, Z.; Greenblatt, M. *J. Solid State Chem.* **1990**, *88*, 278.

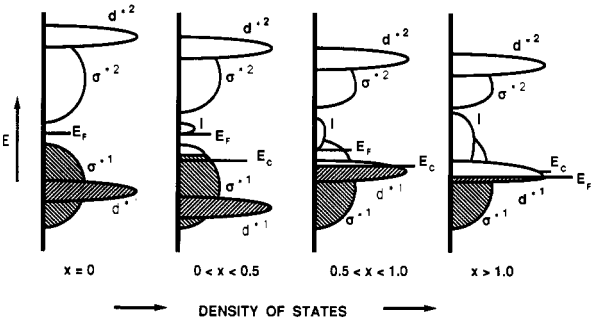

Figure 6. Possible schematic density of states diagram for the σ-bond 3d electrons of $La_{2-x}Sr_xNiO_{4-\delta}$. The $\sigma^{*1}_{x^2-y^2}/\sigma^{*2}_{x^2-y^2}$ bands and the $d^{*1}_{z^2}/d^{*2}_{z^2}$ orbitals are indicated by σ^{*1}/σ^{*2} and d^{*1}/d^{*2}, respectively. E_F is the Fermi level, and E_c is the mobility edge. The shaded area is the occupied band or orbital. The impurity band is indicated by I.

Goodenough[16] proposed a density of states diagram for La_2NiO_4 to explain the metal–nonmetal transition at high temperature (~500 K). In the model, it is proposed that the bands that dominate the transport properties originate from Ni(3d) states of the σ-bonding orbitals of e_g parentage at an octahedral Ni^{2+} ion. Due to tetragonal distortion these orbitals are split to form a $\sigma^*_{x^2-y^2}$ band of itinerant electron states with $d^*_{x^2-y^2}$ parentage and a localized $d^*_{z^2}$ orbital. Large on-site Coulombic repulsion then transforms these two-electron bands/states into four one-electron bands/states: $d^{*1}_{x^2-y^2}$, $d^{*2}_{x^2-y^2}$, and $d^{*1}_{z^2}$, $d^{*2}_{z^2}$. A bandgap forms between $d^{*1}_{x^2-y^2}$ and $d^{*2}_{x^2-y^2}$, which results in a semiconductor or nonmetal for the $x = 0$ material at $T \lesssim 500$ K (see Figure 6).

For the strontium-doped 214 $La_{2-x}Sr_xNiO_{4-\delta}$ system, the evolution of the lattice constants as a function of x may be explained by using the density of states diagram analogous to Goodenough's. Substitution of La^{3+} with Sr^{2+} brings about the oxidation of the square-planar layer needed to maintain charge neutrality. The manifestation of Sr^{2+} substitution is apparent in the crystallographic and electrical resistance data (Figures 1–3 and 5). Each Sr^{2+} can be considered as bringing about the removal of an electron from the highest occupied molecular orbital. Since the HOMOs we are dealing with have antibonding character with respect to the O^{2-} ligands, the electron density distribution in these orbitals will be described as antibonding. Initially, substitution of Sr^{2+} for La^{3+} removes antibonding electrons from the $\sigma^{*1}_{x^2-y^2}$ band because its potential energy is higher than $d^{*1}_{z^2}$ orbitals as a result of the Jahn–Teller distortion of Ni^{3+}. Up to a certain level of x, electron density would be reduced in both the $\sigma^{*1}_{x^2-y^2}$ and $d^{*1}_{z^2}$ orbitals in differing proportions depending upon their relative energies because they are shifting with x. The observations on color changes with composition (Table II) support this view.

For $0 \leq x \leq \sim 0.6$ electrons are removed from the $\sigma^{*1}_{x^2-y^2}$ band. Removal of the antibonding electrons from the $\sigma^{*1}_{y^2-y^2}$ band lessens the interaction of Ni $d^*_{x^2-y^2}$–$Op_{x,y}$–Ni $d^*_{x^2-y^2}$ in the square-planar array, resulting in the increase of the Ni–O bond order and therefore the decrease of the Ni–O distance. The increase in the c parameter comes from more antibonding electrons populated in the axial bond region due to the stabilization of $d^{*1}_{z^2}$ orbital relative to the $\sigma^{*1}_{x^2-y^2}$ band.

As the level of doping increases, this tendency gradually reverses as $x \geq \sim 0.6$. The energy position of the $\sigma^{*1}_{x^2-y^2}$ band shifts downward progressively and the $d^{*1}_{z^2}$ orbital upward. The antibonding electrons redistribute them-

(16) Goodenough, J. B.; Ramasesha, S. *Mater. Res. Bull.* **1982**, *17*, 383.

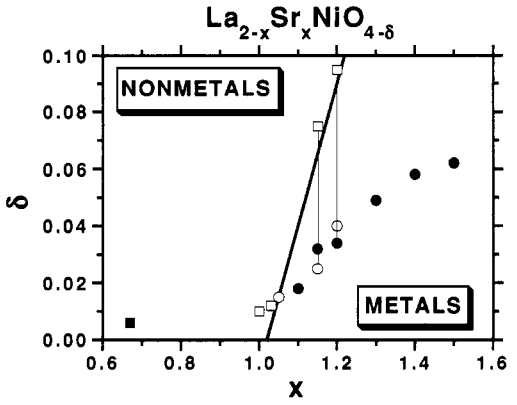

Figure 7. Metal–nonmetal phase diagram for $La_{2-x}Sr_xNiO_{4-\delta}$ in terms of the degree of substitution of La by Sr (x) and the oxygen deficiency δ. All metals are represented by circles and all nonmetals by squares. The values of x for all open symbols are experimentally known, but the corresponding δ values are estimates. Black symbols are experimental points.

selves between the $\sigma^{*1}_{x^2-y^2}$ band and $d^{*1}_{z^2}$ orbital. For $\sim 0.6 < x < 1.0$ electron density is removed from both the $d^{*1}_{z^2}$ orbital and the $\sigma^{*1}_{x^2-y^2}$ band. This results in a decrease in the c lattice parameter and potentially a decrease in the a lattice parameter. However, because the $d^{*1}_{z^2}$ orbital is shifting upward and the $\sigma^{*1}_{x^2-y^2}$ band is shifting downward, the net effect is an increase of the electron density in the $\sigma^{*1}_{x^2-y^2}$ band. This effect would alone cause an increase in the a axis but is nullified when combined with the decrease described above. This causes the a lattice parameter to stay nearly constant.

For $x > 1.0$ the electrons are still removed as in the diagram described above. The $d^{*1}_{z^2}$ orbital keeps shifting upward and hence decreasing the c axis, while the $\sigma^{*1}_{x^2-y^2}$ band is shifting downward and increasing the a axis up to $x = 1.3$ due to more relative antibonding electron density. Notice that in this range from a formal valence point of view $La_{2-x}Sr_xNiO_{4-\delta}$ becomes a Ni^{3+}/Ni^{4+} mixed valent system instead of Ni^{2+}/Ni^{3+}. In the range $1.3 \leq x \leq 1.5$ removal of antibonding electrons from the two e_g^* MOs eventually occurs mainly in the $\sigma^{*1}_{x^2-y^2}$ band because of the depletion of the electron density in the $d^{*1}_{z^2}$ orbital. Consequently, the a axis decreases and the c axis begins to level off.

As x increases, disorder is introduced due to the random nature of the Sr^{2+} in the A sites of the A_2BO_4 lattice and nonzero δ. This is evident by the $\exp[T^{-1/4}]$ behavior in the conductivity at low temperature in the nonmetallic regime, which is indicative of variable range hopping in disordered systems. As a result a mobility edge is formed. With the states localized at the top of the band no metallic material is produced for small x. The disorder consequently causes the formation of an impurity band in the band gap. Increase in x also causes a broadening of all other bands. In addition, the replacement of La^{3+} by the less acidic Sr^{2+} decreases the competition for the $O(2p_\pi)$ electrons and this leads to specific broadening of the Ni(3d) bands.[17] For sufficient Sr^{2+} doping level ($x \geq \sim 1.05$) the impurity band overlaps with the $\sigma^{*1}_{x^2-y^2}$ band and this leads to metallic conduction. It is conceivable that the metal–nonmetal transition is of the Anderson type.[18]

Nonstoichiometry of oxygen is usually found in the $La_2NiO_{4+\delta}$. Excess Ni^{3+} is also found in the $La_{2-x}Sr_xNiO_{4-\delta}$ for $0 \leq x \leq \sim 0.6$. This excess oxygen gradually decreases with increasing x and becomes a deficiency as $x > \sim 0.6$ (Table II and ref 13). The transport properties are dependent on the atmosphere used during preparation of the samples and their thermal history.[19] As shown in Figure 4 the metallic character of materials with $x = 1.5$ and 1.20 becomes nonmetallic by heating the samples in argon at 1000 °C, which is interpreted as a loss of oxygen or chemical reduction due to dissociation. Their metallic properties are restored upon heating in oxygen at 1000 °C which is interpreted as oxidation or a decrease in δ. The stoichiometry of oxygen are known to be critical in the 123 and 214 cuprates.[20,21] This is consistent with the view that the indirect cation–anion–cation interactions mediated through the anion p_π orbitals are by no means negligible.

In conclusion, the conducting behavior of the materials represented by $La_{2-x}Sr_xNiO_{4-\delta}$ can be controlled by the doping level of Sr^{2+} and the stoichiometry of oxygen, the variation of the lattice constants is a function of a small Jahn–Teller distortion and of the relative position in energy of the two e_g^* MOs. Nonmetallic conducting behavior observed for $x < 1.0$ and the metallic type observed for $x > 1.1$ coupled with the major effects on conductivity by minor changes in oxygen stoichiometry for the composition $x = 1.15$ and 1.20 lead us to propose the phase diagram shown in Figure 7. The transition boundary is given by the equation $\delta = 0.5x - 0.51$, which corresponds, within the formalism used in this paper, to an average Ni valence of ~ 3.02.

Following the preparation of this paper the work of Sreedhar and Rao[22] on $La_{2-x}Sr_xNiO_{4-\delta}$ (x up to 1.2) was published. Both studies complement each other. They examine one composition where $x > 1.0$ and conclude on the basis of its room-temperature conductivity that it is metallic. Sreedhar and Rao also present electrical conductivity measurements as a function of temperature (300–800 K) and magnetic susceptibility measurements for compositions below $x = 1.0$. Our work has focused on several compositions above $x = 1.0$ as well as those below that value, on the electrical conductivity (resistance as a function of temperature) from 300 to about 4 K for these materials, and on the sensitivity of the electrical conductivity to oxygen vacancies.

Acknowledgment. We are grateful to Professor C. L. Chien for the use of the X-ray diffraction equipment. We are also grateful to W. R. Grace and Co. for supplying the high-temperature furnace used in this research. This work is supported in part by the NSF Solid State Program Grant DMR-8921071.

(17) Egdell, R. G.; Harrison, M. R.; Hill, M. D.; Porte, L.; Wall, G. *J. Phys. C: Solid State Phys.* **1984**, *17*, 2889.

(18) Mott, N. F. *Metal-Insulator Transition*, 2nd ed.; Taylor and Francis: London, 1990.

(19) Odier, P.; Nigara, Y.; Coutures, J. *J. Solid State Chem.* **1985**, *56*, 32.

(20) Grant, P. M.; Parkin, S. S. P.; Lee, V. Y.; Engler, E. M.; Ramirez, M. L.; Vazquez, J. E.; Lim, G.; Jacowitz, R. D.; Greene, R. L. *Phys. Rev. Lett.* **1987**, *58*, 2482.

(21) Johnston, D. C.; Jacobson, A. J.; Newsam, J. M.; Lewandowski, J. T.; Goshorn, D. P.; Xie, D.; Yelon, W. B. *Chemistry of High-Temperature Superconductors*; American Chemical Society: Washington, DC, 1987.

(22) Sreedhar, K.; Rao, C. N. R. *Mater. Res. Bull.* **1990**, *25*, 1235.